GEOPHYSICS, VOL. 76, NO. 4 (JULY-AUGUST 2011); P. S165–S175, 8 FIGS.
10.1190/1.3590214

Reducing two-way splitting error of FFD method in dual domains

Jin-Hai Zhang[1] and Zhen-Xing Yao[1]

ABSTRACT

The Fourier finite-difference (FFD) method is very popular in seismic depth migration. But its straightforward 3D extension creates two-way splitting error due to ignoring the cross terms of spatial partial derivatives. Traditional correction schemes, either in the spatial domain by the implicit finite-difference method or in the wavenumber domain by phase compensation, lead to substantially increased computational costs or numerical difficulties for strong velocity contrasts. We propose compensating the two-way splitting error in dual domains, alternately in the spatial and wavenumber domains via Fourier transform. First, we organize the expanded square-root operator in terms of two-way splitting FFD plus the usually ignored cross terms. Second, we select a group of optimized coefficients to maximize the accuracy of propagation in both inline and crossline directions without yet considering the diagonal directions. Finally, we further optimize the constant coefficient of the compensation part to further improve the overall accuracy of the operator. In implementation, the compensation terms are similar to the high-order corrections of the generalized-screen method, but their functions are to compensate the two-way splitting error rather than the expansion error. Numerical experiments show that optimized one-term compensation can achieve nearly perfect circular impulse responses and the propagation angle with less than 1% error for all azimuths is improved up to 60° from 35°. Compared with traditional single-domain methods, our scheme can handle lateral velocity variations (even for strong velocity contrasts) much more easily with only one additional Fourier transform based on the two-way splitting FFD method, which helps retain the computational efficiency.

INTRODUCTION

One-way wave-equation depth migration is an important tool when imaging complex media (Claerbout, 1985; Etgen et al., 2009). Many methods have been developed during the last three decades, such as the finite-difference method (Claerbout, 1985), the Fourier method (Gazdag, 1978), and the dual-domain method (e.g., Stoffa et al., 1990; Ristow and Rühl, 1994; Wu, 1994; Jin et al., 1999; de Hoop et al., 2000; Le Rousseau and de Hoop, 2001; Xie and Wu, 2001; Wu, 2003). As a dual-domain method, the Fourier finite-difference (FFD) method (Ristow and Rühl, 1994) combines the advantages of the Fourier method and the finite-difference method by cascading an implicit finite-difference correction to the split-step Fourier method (see Zhang et al. (2009b) for a detailed comparison between the FFD method and the Fourier method). The FFD method is very popular in imaging complex structures because it can handle strong lateral velocity variations and steep dips.

Unfortunately, the FFD method's direct 3D extension is extremely costly because 3D implicit finite-difference correction involves solving large sparse matrices (Claerbout, 1985; Li, 1991). A practical approach is to sequentially split the 3D implicit finite-difference correction into two cascaded 2D operators along the inline and crossline directions, which is called a two-way splitting technique (Brown, 1983) or an alternating-direction-implicit scheme (Peaceman and Rachford, 1955; Wachspress and Habetler, 1960; Douglas, 1962). Although the two-way splitting technique affords high computational efficiency, it introduces large phase errors (called two-way splitting error or azimuthal anisotropy) for wide-angle propagations at 45° and 135° azimuths. This azimuthal anisotropy causes the depth slice of impulse response in 3D homogeneous media (with reference velocity smaller than real velocity) to not show a perfect circle but a "smoothed diamond"; that is, the wave propagation speed in diagonal directions appears to be slower than that in inline and crossline directions. In addition, this error

Manuscript received by the Editor 29 September 2010; revised manuscript received 30 December 2010; published online 9 June 2011.
[1]Chinese Academy of Sciences, Institute of Geology and Geophysics, Beijing, China. E-mail: zjh@mail.igcas.ac.cn; yaozx@mail.igcas.ac.cn.
© 2011 Society of Exploration Geophysicists. All rights reserved.

Downloaded 10 Jun 2011 to 159.226.119.199. Redistribution subject to SEG license or copyright; see Terms of Use at http://segdl.org/

becomes more apparent with increasing dip angles and increasing velocity contrast (Zhang et al., 2008). Consequently, the two-way splitting FFD method has low accuracy in diagonal directions, especially for steep dips in 3D strongly heterogeneous media. The two-way splitting error may lead to incorrect positioning or lack of images when imaging steep structures, especially in the presence of strong velocity contrasts (Claerbout, 1985; Wang, 2001).

Several approaches have been proposed to deal with the two-way spitting error. One way is to avoid the two-way spitting error by directly solving the banded linear systems arising from the 3D downward continuation equations. Rickett et al. (1998) propose the helical boundary conditions, which invert the 2D convolution matrix with an equivalent 1D filter operation. Fei and Etgen (2002) propose the domain decomposition method, which solves the 2D convolution matrix in multiple subdomains. Another way, which is very popular in practice, is to apply the two-way splitting technique first and then append correction terms to compensate the two-way splitting error. There are several different kinds of implementations, as we outline below.

Graves and Clayton (1990) derive a phase-correction filter in the spatial domain by solving a cascade of tridiagonal matrix systems. This method works but its computational cost doubles compared to the cost of the two-way splitting finite-difference method. Li (1991) proposes an error-compensation equation using the phase-shift method for laterally homogeneous media. Phase shift plus interpolation (Gazdag and Sguazzero, 1984) can be used to handle heterogeneous media with potentially substantial increase in computational cost. Collino and Joly (1995) and Ristow and Rühl (1997) apply four-way splitting to obtain a circular response; that is, two additional extrapolations along diagonal directions are cascaded after the two-way splitting. Although a nearly perfect response could be obtained, the computational cost is doubled. In addition, the finite-difference solver in the diagonal directions encounters more serious numerical dispersion because the spatial interval is increased by a factor of $\sqrt{2}$ and additional computations are required for wavefield interpolations in the presence of $dx \neq dy$ (Ristow and Rühl, 1997). Biondi (2002) suggests performing FFD plus interpolation to reduce azimuthal anisotropy. The computational cost is at least doubled. Wang (2001) proposes a wavenumber-domain interpolation scheme to pick up the ignored cross terms of inline and crossline wavenumbers. Zhang et al. (2008) introduce Wang's scheme (2001) to the FFD operator and reduce the computational cost by optimizing the algorithm structure. However, as a purely wavenumber-domain method, Wang's scheme has difficulty selecting a proper velocity to account for strong lateral heterogeneous media. Therefore, a new method with high accuracy and computational efficiency is still in demand to reduce the two-way splitting error of the FFD method.

Dual-domain methods handle spatial and wavenumber variables in spatial and wavenumber domains alternatively, where wavefields are shuttled between space and wavenumber domains using Fourier transforms. This method is widely used in constructing new migration methods (e.g. Stoffa et al., 1990; Ristow and Rühl, 1994; Wu, 1994; Jin et al., 1999; de Hoop et al., 2000; Le Rousseau and de Hoop, 2001; Wu, 2003; Liu and Zhang, 2006; Zhang and Liu, 2007; Zhang et al., 2010). In this paper, we apply the dual-domain method to compensate the two-way splitting error of the FFD method. First, we organize the expanded square-root operator in terms of two-way splitting FFD plus usually ignored cross terms of inline and crossline wavenumbers. Second, we rearrange cross terms using variable separation. Then, we implement the compensation using dual-domain method by Fourier transforms. Finally, we optimize the constant coefficients to reduce the number of terms added. Only one additional Fourier transform is required in our scheme compared to the traditional two-way splitting FFD method. Numerical results show perfect circles in the depth slice of 3D impulse response. The accurate dip angle using a relative error cutoff of 1% is not smaller than 60° for all azimuths, including diagonal, inline, and crossline directions.

It is easy to extend our dual-domain compensation scheme from the traditional two-way splitting FFD method because the FFD method is a dual-domain method already. The added terms are implemented in a similar manner to the high-order terms of the generalized-screen method (de Hoop et al., 2000), but their function is to reduce the two-way splitting error of the FFD method rather than to reduce the expansion error of the square-root operator. In implementation, our scheme can be regarded as a natural combination of the two-way splitting FFD method and the high-order generalized-screen method. It handles lateral velocity variations by separation of variables in dual domains as does the generalized-screen method (de Hoop et al., 2000). Compared with purely wavenumber-domain methods (such as Li's compensation [1991] and Wang's scheme [2001]), our scheme can handle lateral velocity variations (even for strong velocity contrasts) much more easily with only one additional compensation term. Compared with the finite-difference correction in the spatial domain, such as the four-way splitting, our scheme can handle nonsquare grids easily and has less numerical dispersion for coarse grids.

METHODOLOGY

Two-way splitting FFD method

The downward extrapolation wave equation for 3D one-way depth migration in the frequency domain reads (Claerbout, 1985)

$$\frac{\partial P(x,y,z;\omega)}{\partial z} = i\kappa_z P(x,y,z;\omega), \tag{1}$$

with the square-root operator defined as $\kappa_z = \sqrt{\omega^2/v^2 + \partial^2/\partial x^2 + \partial^2/\partial y^2}$, where $v \equiv v(x,y,z)$ is the velocity, $i = \sqrt{-1}$ is the imaginary unit, ω is the circular frequency, and $P(x,y,z;\omega)$ is the pressure in the frequency domain. The formal solution of equation 1 is

$$\begin{aligned} P(x,y,z+\Delta z;\omega) &= \exp\left(i\int_z^{z+\Delta z} \kappa_z(x,y,z;\omega)dz\right)P(x,y,z;\omega) \\ &\approx \exp(i\kappa_z \Delta z)P(x,y,z;\omega), \end{aligned} \tag{2}$$

where Δz is the thickness of the horizontal thin slab, or, depth interval.

According to relations $\partial^2/\partial x^2 \Leftrightarrow -k_x^2$ and $\partial^2/\partial y^2 \Leftrightarrow -k_y^2$, the square-root operator can be translated into a vertical wavenumber (also called a dispersion relationship) as follows:

$$k_z = \sqrt{\frac{\omega^2}{v^2} - k_x^2 - k_y^2}, \tag{3}$$

Downloaded 10 Jun 2011 to 159.226.119.199. Redistribution subject to SEG license or copyright; see Terms of Use at http://segdl.org/

where k_x and k_y are horizontal wavenumbers along inline and crossline directions, respectively. The vertical wavenumber $k_z = \sqrt{\omega^2/v^2 - k_x^2 - k_y^2}$ for real velocity $v(x,y,z)$ can be expanded by Taylor expansion as

$$k_z = \frac{\omega}{v}\sum_{n=0}^{\infty} a_n \left[\frac{v^2}{\omega^2}\left(k_x^2 + k_y^2\right)\right]^n, \tag{4}$$

where a_n are binomial coefficients with the first five being $a_0 = 1$, $a_1 = -1/2$, $a_2 = -1/8$, $a_3 = -1/16$, and $a_4 = -5/128$. Similarly, the vertical wavenumber $k_z^0 = \sqrt{\omega^2/v_0^2 - k_x^2 - k_y^2}$ for the reference velocity $v_0 \equiv v_0(z)$ can be expanded as

$$k_z^0 = \frac{\omega}{v_0}\sum_{n=0}^{\infty} a_n \left[\frac{v_0^2}{\omega^2}\left(k_x^2 + k_y^2\right)\right]^n. \tag{5}$$

Substituting equations 4 and 5 into identical equation $k_z = k_z^0 + \left(k_z - k_z^0\right)$ and using a continued-fraction expansion (Claerbout, 1985), we obtain the 3D FFD operator (Ristow and Rühl, 1994; Biondi, 2002)

$$k_z \approx k_z^0 + \left(\frac{\omega}{v} - \frac{\omega}{v_0}\right) - \frac{\beta\left(k_x^2 + k_y^2\right)}{1 - \alpha\left(k_x^2 + k_y^2\right)}, \tag{6}$$

where $\alpha = 0.25\left(v^2 + vv_0 + v_0^2\right)/\omega^2$ and $\beta = 0.5(v - v_0)/\omega$. In fact, we can obtain equation 6 in another way by two steps — deriving a 2D FFD operator first and then extending it to a 3D case by simply replacing k_x^2 with $k_x^2 + k_y^2$.

The formal solution of one-way wave equation can be decomposed for laterally varying media into three cascaded equations:

$$P'(x,y,z+\Delta z;\omega) = F^-\left\{\exp\left(ik_z^0\Delta z\right)F^+[P(x,y,z;\omega)]\right\}, \tag{7}$$

$$P''(x,y,z+\Delta z;\omega) = \exp\left[i\left(\frac{\omega}{v} - \frac{\omega}{v_0}\right)\Delta z\right]P'(x,y,z+\Delta z;\omega), \tag{8}$$

and

$$\frac{\partial P''(x,y,z+\Delta z;\omega)}{\partial z} = \frac{i\beta\left(\frac{\partial^2}{\partial x^2} + \frac{\partial^2}{\partial y^2}\right)}{1 + \alpha\left(\frac{\partial^2}{\partial x^2} + \frac{\partial^2}{\partial y^2}\right)}P''(x,y,z+\Delta z;\omega), \tag{9}$$

where F^+ and F^- denote 2D forward and inverse Fourier transforms along horizontal space, respectively. Equation 7 performs the phase shift for the reference velocity in the wavenumber domain (Gazdag, 1978), equation 8 performs the time-delay correction for slowness perturbations in the spatial domain (Stoffa et al., 1990), and equation 9 handles the high-order corrections for large velocity contrasts and wide-angle propagations using the implicit finite-difference method (Ristow and Rühl, 1994).

The direct implementation of the 3D implicit finite-difference scheme in the third term (i.e., equation 9) requires solving large sparse-matrix equations, which is extremely expensive. A practical way is to further split it into two independent 2D operators by ignoring the cross terms of k_x^2 and k_y^2 as follows:

$$\frac{\beta\left(k_x^2 + k_y^2\right)}{1 - \alpha\left(k_x^2 + k_y^2\right)} \approx \frac{\beta k_x^2}{1 - \alpha k_x^2} + \frac{\beta k_y^2}{1 - \alpha k_y^2}. \tag{10}$$

This approach is called the two-way splitting technique (Brown, 1983) or the alternating-direction-implicit (ADI) scheme (Douglas, 1962). Thus, the two-way splitting FFD operator is approximated as

$$k_z \approx k_z^0 + \left(\frac{\omega}{v} - \frac{\omega}{v_0}\right) - \frac{\beta k_x^2}{1 - \alpha k_x^2} - \frac{\beta k_y^2}{1 - \alpha k_y^2}. \tag{11}$$

The last two terms in equation 11 can be efficiently solved as two cascaded tridiagonal systems. In implementation, equation 9 is further split into two cascaded equations as follows:

$$\frac{\partial P''(x,y,z+\Delta z;\omega)}{\partial z} = \frac{i\beta\frac{\partial^2}{\partial x^2}}{1 + \alpha\frac{\partial^2}{\partial x^2}}P''(x,y,z+\Delta z;\omega) \tag{12}$$

and

$$\frac{\partial P'''(x,y,z+\Delta z;\omega)}{\partial z} = \frac{i\beta\frac{\partial^2}{\partial y^2}}{1 + \alpha\frac{\partial^2}{\partial y^2}}P'''(x,y,z+\Delta z;\omega). \tag{13}$$

Taking the wavefields $P(x,y,z;\omega)$ as initial conditions at the depth level z, we can extrapolate them to the depth level $z + \Delta z$ by sequentially solving equations 7, 8, 12, and 13. Taking the output wavefields $P'''(x,y,z+\Delta z;\omega)$ as initial conditions at the depth level $z + \Delta z$, we can obtain wavefields at the depth level $z + 2\Delta z$. Repeating this procedure from the upper surface downward to the bottom of a 3D model, we could obtain wavefields at all depth levels.

The two-way splitting technique causes significant error for wide-angle propagations along the oblique directions and is harmful for imaging steep dips. In the following two sections, we present a new method to reduce the two-way splitting error with high accuracy and computational efficiency.

Compensation in dual domains

Substituting both equations 4 and 5 into the equation $k_z = k_z^0 + \left(k_z - k_z^0\right)$ and rearranging the coefficients of k_x^2 and k_y^2, we obtain

$$k_z = k_z^0 + \sum_{n=0}^{\infty} a_n d_n k_x^{2n} + \sum_{n=0}^{\infty} a_n d_n k_y^{2n} + \sum_{n=2}^{\infty} n a_n d_n \sum_{i=1}^{n-1} k_x^{2i} k_y^{2n-2i}, \tag{14}$$

where $d_n = v^{2n-1}/\omega^{2n-1} - v_0^{2n-1}/\omega^{2n-1}$. It is well known that the 2D FFD operator has very high accuracy. Thus, we truncate to $n = 2$ and apply continued-fraction expansion to k_x^{2n} and k_y^{2n}, respectively:

$$k_z \approx k_z^0 + \left(\frac{\omega}{v} - \frac{\omega}{v_0}\right) - \frac{\beta k_x^2}{1 - \alpha k_x^2} - \frac{\beta k_y^2}{1 - \alpha k_y^2} + \sum_{n=2}^{\infty} n a_n d_n \sum_{i=1}^{n-1} k_x^{2i} k_y^{2n-2i}. \tag{15}$$

Downloaded 10 Jun 2011 to 159.226.119.199. Redistribution subject to SEG license or copyright; see Terms of Use at http://segdl.org/

The first four terms constitute the traditional two-way splitting FFD operator (i.e., equation 11) and the last term is the usually ignored cross term. It is obvious that the cross terms emerge from $n = 2$.

The first-order compensation reads

$$c_1 = -\frac{1}{4}\left(\frac{v^3}{\omega^3} - \frac{v_0^3}{\omega^3}\right)k_x^2 k_y^2 \tag{16}$$

and the second-order compensation reads

$$c_2 = -\frac{3}{16}\left(\frac{v^5}{\omega^5} - \frac{v_0^5}{\omega^5}\right)\left(k_x^2 k_y^4 + k_x^4 k_y^2\right). \tag{17}$$

It is difficult for the finite-difference method to handle terms containing products of k_x^2 and k_y^2. Consequently, we handle these terms using a Fourier scheme to compensate two-way splitting errors. In implementation, equations 16 and 17 correspond to the following equations, respectively:

$$P_c'(x, y, z + \Delta z; \omega) = \exp(ic_1\Delta z)P'''(x, y, z + \Delta z; \omega) \tag{18}$$

and

$$P_c''(x, y, z + \Delta z; \omega) = \exp(ic_2\Delta z)P_c'(x, y, z + \Delta z; \omega), \tag{19}$$

where $P'''(x, y, z + \Delta z; \omega)$ are the output wavefields of the traditional two-way splitting FFD method (see equation 13) and $P_c'(x, y, z + \Delta z; \omega)$ and $P_c''(x, y, z + \Delta z; \omega)$ are the output wavefields of the first- and second-order corrections, respectively. Unfortunately, the spatial variables are not explicitly separated from the wavenumber variables because they are coupled as an exponent of a complex exponential function (see equation 18 or 19). Another Taylor expansion, $e^{ix} \approx 1 + ix$, is required for the exponential function to completely separate the spatial and wavenumber variables (de Hoop et al., 2000); that is, compensation equations 18 and 19 should be further approximated, respectively, as

$$P_c'(x, y, z + \Delta z; \omega) \approx (1 + ic_1\Delta z)P'''(x, y, z + \Delta z; \omega) \tag{20}$$

and

$$P_c''(x, y, z + \Delta z; \omega) \approx (1 + ic_2\Delta z)P_c'(x, y, z + \Delta z; \omega). \tag{21}$$

The two-way splitting FFD method accurately handles wave propagation except at wide propagation angles in the presence of strong lateral velocity contrasts. Thus, the high-order terms (i.e., equations 20 and 21) only handle wide-angle corrections (usually beyond 45°) primarily in diagonal directions. We assume the exponents $ic_1\Delta z$ and $ic_2\Delta z$ are small enough to guarantee the suitability of Taylor expansion used in equations 20 and 21. However, a direct implementation of equations 20 and 21 will encounter stability problems. De Hoop et al. (2000) suggest a normalization operator $\mathcal{N}$ to stabilize the wavefield extrapolation and to reduce the phase error caused by the Taylor expansion, which reads

$$N(1 + p + iq) = \exp(iq)\left|1 + \frac{p}{1 + iq}\right|^{-1}\left(1 + \frac{p}{1 + iq}\right), \tag{22}$$

where p and q denote the real part and imaginary part of a complex number, respectively.

The spatial variables associated with v are handled in the spatial domain whereas the wavenumber variables associated with $k_x k_y$ are handled in the wavenumber domain. Fast Fourier transforms are needed to shuttle wavefields between spatial and wavenumber domains, with forward fast Fourier transform transforming wavefields from the spatial domain to the wavenumber domain and inverse fast Fourier transform transforming wavefields from the wavenumber domain to the spatial domain. Therefore, detailed wavefield extrapolation procedures for compensation equations 20 and 21 are

$$\bar{P}_c'(k_x, k_y) = F^+[P'''(x, y)] \times N\left\{1 + \frac{i\Delta z k_x^2 k_y^2 F^+[2a_2 d_2 P'''(x, y)]}{F^+[P'''(x, y)]}\right\} \tag{23}$$

and

$$P_c''(x,y) = F^-\left[\bar{P}_c'(k_x,k_y)\right] \times N\left\{1 + \frac{i\Delta z 3a_3 d_3 F^-\left[\left(k_x^2 k_y^4 + k_x^4 k_y^2\right)\bar{P}_c'(k_x,k_y)\right]}{F^-\left[\bar{P}_c'(k_x,k_y)\right]}\right\}, \tag{24}$$

where $\bar{P}_c'(k_x, k_y)$ are the wavenumber-domain wavefields after applying the first-order correction. Refer to Zhang et al. (2009a) for a very similar algorithm, which presents the detailed pseudocode of the generalized-screen method. Expressions of $z + \Delta z$ and ω are omitted in wavefield variables for brevity. As in the generalized-screen method, each additional term of compensation requires an additional forward Fourier transform by revising the sequence of extrapolations (see pseudo code in Zhang et al., 2009a). Thus, two-term compensation requires four 2D Fourier transforms and two implicit finite-difference solutions for wavefield extrapolation at each depth level. Compared with the two-way splitting FFD method, one-term compensation needs one more Fourier transform and two-term compensation needs two more Fourier transforms.

Global optimization by simulated annealing

Although two-term compensation works well to produce an almost perfect circle, its computational cost is relatively high. In addition, its accurate propagation angle, the smallest dip angle that just begins to reach 1% phase error as a function of azimuth, is relatively low. We hope to minimize the increasing of computational cost based on the two-way splitting FFD method by using only one term; that is, only one more Fourier transform is needed rather than two more Fourier transforms.

Optimizing constant coefficients of an operator can further improve the accurate propagation angle under a given error threshold while retaining the algorithm structure and the computational cost (Lee and Suh, 1985; Ristow and Rühl, 1994; Xie and Wu, 1999; Huang and Fehler, 2000; Liu and Zhang, 2006; Zhang and Liu, 2007; Zhu et al., 2008; Zhang et al, 2010). There are two kinds of optimization methods: local optimization scheme and global optimization scheme (Huang and Fehler, 2000). The local optimization scheme needs to optimize constant coefficients for different velocity ranges among all depth slices. It produces a list of optimization coefficients stored in memory and requires a table lookup for each depth slice during

Downloaded 10 Jun 2011 to 159.226.119.199. Redistribution subject to SEG license or copyright; see Terms of Use at http://segdl.org/

wavefield extrapolation. In contrast, the global optimization scheme only needs to optimize constant coefficients for the universal velocity range of the whole 3D velocity; thus, it has only one group of optimized coefficients for a given velocity model and is convenient for applications.

There are two kinds of error for two-way splitting FFD operators: expansion error and two-way splitting error (Zhang et al., 2009b). The error in inline and crossline directions is purely expansion error; the error in other directions (including diagonal directions) consists of both. Applying a global optimization scheme (Huang and Fehler, 2000) and a multiparameter scheme, Zhu et al. (2008) greatly reduce the expansion error of the FFD method. Under a relative error of 1%, the accurate propagation angle is no lower than 75° for most velocity functions encountered in practice. Although optimizing constant coefficients can significantly reduce the expanded error, it offers minimal help for reducing two-way splitting error without considering the compensation terms (Zhang et al., 2008). We hope to significantly reduce the two-way splitting error by optimizing constant coefficients of the dual-domain compensation. One way is to optimize all constant coefficients of the whole FFD operator simultaneously, but this leads to too many variables to be optimized. Another way is to optimize constant coefficients of the two-way splitting FFD method and the one-term compensation in sequence. The latter is more attractive because of its simplicity. In addition, it is helpful to improve the convergence of our optimization procedure. In this paper, we adopt the optimized coefficients obtained by Zhu et al. (2008) to guarantee the wide-angle precision in inline and crossline directions. Next, we will concentrate on optimizing the coefficients of the compensation term.

We represent transversal wavenumbers in terms of azimuth angle φ and of dip angle θ as (Claerbout, 1985; Li, 1991)

$$k_x = \frac{\omega}{v}\sin\theta\cos\varphi \quad \text{and} \quad k_y = \frac{\omega}{v}\sin\theta\sin\varphi. \tag{25}$$

Then, the relative phase error can be defined as

$$R(\varphi,\theta,p) = \frac{|\tilde{k}_z - k_z|}{k_z} \times 100\%, \tag{26}$$

where the accurate vertical wavenumber is $k_z = \omega\cos\theta/v$, the approximated vertical wavenumber $\tilde{k}_z$ of the two-way splitting FFD method is given in equation 11, and the approximated vertical wavenumber $\tilde{k}_z$ of the two-way splitting FFD plus dual-domain compensation is given in equation 15. The velocity contrast is defined as $(v-v_0)/v\times 100\% = (1-p)\times 100\%$. A small velocity contrast denotes weak lateral velocity variations and a large value denotes strong lateral velocity variations.

We rewrite the operator of second-order compensation as follows:

$$k_z \approx k_z^{\oplus} - \frac{1}{4}\left(\frac{v^3}{\omega^3} - \frac{v_0^3}{\omega^3}\right)k_x^2k_y^2 - \frac{3}{16}\left(\frac{v^5}{\omega^5} - \frac{v_0^5}{\omega^5}\right)\left(k_x^2k_y^4 + k_x^4k_y^2\right), \tag{27}$$

where the first term of equation 27 (i.e., symbol $k_z^{\oplus}$) denotes the two-way splitting FFD propagator as shown in equation 11, the second term (i.e., $-1/4\left(v^3 - v_0^3\right)k_x^2k_y^2/\omega^3$) is the first-order compensation term, and the third term (i.e., $-3/16\left(v^5 - v_0^5\right)\left(k_x^2k_y^4 + k_x^4k_y^2\right)\Big/\omega^5$) is the second-order compensation term. If we truncate to the first-order compensation and optimize its constant coefficient, the accurate dip angle is still limited (only about 55°). To further improve the accuracy, we apply a continued-fraction approximation (Claerbout, 1985) as follows:

$$\begin{aligned} k_z &\approx k_z^{\oplus} - \frac{1}{4}\left(\frac{v^3}{\omega^3} - \frac{v_0^3}{\omega^3}\right)k_x^2k_y^2\left[1 + \frac{3}{4}\left(\frac{v^5}{\omega^5} - \frac{v_0^5}{\omega^5}\right)\left(k_x^2 + k_y^2\right)\right] \\ &\approx k_z^{\oplus} - \frac{\frac{1}{4}\left(\frac{v^3}{\omega^3} - \frac{v_0^3}{\omega^3}\right)k_x^2k_y^2}{1 - \frac{3}{4\omega^2}\frac{v^5 - v_0^5}{v^3 - v_0^3}\left(k_x^2 + k_y^2\right)}. \end{aligned} \tag{28}$$

Considering relations in equation 25, we can further simplify to

$$\begin{aligned} k_x^2 + k_y^2 &= \frac{\omega^2}{v^2}\sin^2\theta\cos^2\varphi + \frac{\omega^2}{v^2}\sin^2\theta\sin^2\varphi \\ &= \frac{\omega^2}{v^2}\sin^2\theta\left(\cos^2\varphi + \sin^2\varphi\right) \\ &= \frac{\omega^2}{v^2}\sin^2\theta. \end{aligned} \tag{29}$$

As a higher-order correction after the two-way splitting FFD operator, the compensation term comes into effect only if the spitting error is significant. On the other hand, the compensation term is useless when the total error of the expanded square-root is too large. That is, the contribution of the compensation term takes effect only for a certain range of dip angles (e.g., 40°∼70°). To simplify the compensation as a first-order compensation, we set $\sin^2\theta$ in equation 29 to be a constant f_0. Therefore, the modified first-order compensation term becomes

$$k_z \approx k_z^{\oplus} - \frac{\frac{1}{4}\left(\frac{v^3}{\omega^3} - \frac{v_0^3}{\omega^3}\right)k_x^2k_y^2}{1 - \frac{3}{4}\frac{v^5 - v_0^5}{v^5 - v_0^3v^2}f_0}. \tag{30}$$

We set the two constant coefficients in equation 30 as constants to be optimized, i.e.,

$$k_z \approx k_z^{\oplus} - \frac{f_1\left(\frac{v^3}{\omega^3} - \frac{v_0^3}{\omega^3}\right)k_x^2k_y^2}{1 - f_2\frac{v^5 - v_0^5}{v^5 - v_0^3v^2}}. \tag{31}$$

This approximation can further improve the accuracy after optimization while keeping the computational cost constant.

Like the globally optimized scheme (Huang and Fehler, 2000), we divide the practical range of $[1, 1/p_{\min}]$ with a uniform interval of 0.1, where $p_{\min} = \min[v_0/v]$. The constant coefficients in the compensation part (i.e., equation 31) are set to be coefficients to be optimized over $[-1, 1]$. We employ the simulated annealing algorithm (Kirkpatrick et al., 1983) to minimize the percentage relative error of the approximated vertical wavenumber k_z, according to the object function (i.e., equation 26). Over the range of $p \in [1/3, 1]$, under the relative error of 1%, the optimized coefficients of globally optimized two-way splitting FFD method (see Zhu et al., 2008) where $\alpha = (g_1v^2 + g_2vv_0 + g_3v_0^2)/\omega^2$ and $\beta = g_0(v - v_0)/\omega)$ are $g_0 = 0.4403352$, $g_1 = 0.4638829$, $g_2 = 0.1855499$, and $g_3 = 0.2343113$, and the optimized coefficients in the compensation part are $f_1 = 0.4462594$ and $f_2 = 0.3176515$.

Downloaded 10 Jun 2011 to 159.226.119.199. Redistribution subject to SEG license or copyright; see Terms of Use at http://segdl.org/

Relative error analyses

Figure 1 shows the relative error versus azimuth angle at two given dip angles: 45° (see thin lines) and 60° (see bold lines). For each method, the error is larger above the line than the given relative error of 1%. Below the line, the error is smaller. The velocity contrast $(v–v_0)/v\times100\%$ used in this figure is of 70%, which corresponds to a very strong lateral velocity variation. Because the azimuth anisotropy is periodic over the whole azimuth range of $[0°, 360°]$, only the azimuth angles within $[0°, 90°]$ are shown.

The two-way splitting FFD method has a highly unbalanced error distribution among various azimuth angles. The highest accuracy occurs in the inline and crossline directions (i.e., $0°/90°$) and the lowest accuracy occurs in diagonal directions (i.e., 45°). For a dip angle of 45°, the maximum error in inline and crossline directions is under 1%, whereas the maximum error in diagonal directions is about 4% (see the lower dashed thin line). For a dip angle of 60°, the maximum error in inline and crossline directions is only about 6% whereas the maximum error in diagonal directions is about 17% (see the upper dashed bold line). After using our first-order compensation, the azimuthal anisotropy is greatly reduced, whereas the accuracy in the inline and crossline directions is retained (see the dot-dashed lines). For example, the maximum error for a dip angle of 60° is reduced to 10% from 17%. But this error is still much larger than the maximum error of 6% in inline and crossline directions. After using our second-order compensation, the azimuthal anisotropy is almost completely reduced since the error is almost equal for various azimuth angles (see the long dashed lines). The maximum error for a dip angle of 60° is reduced to 6% from 17%. The maximum error for a dip angle of 45° is reduced to 1% from 4%. However, note that the maximum error is still 6% after using second-order compensation for a dip angle of 60°. This means we still could not obtain an accurate image for steep dips. In addition, the second-order compensation needs two additional Fourier transforms; the consequent increase of computational cost is fairly large.

The optimized first-order compensation requires only one additional Fourier transform after the two-way splitting FFD method, the same as the first-order compensation. But its maximum error is always under 1% either for a dip angle of 45° or 60° (see the solid lines in Figure 1). Although its error distribution is again unbalanced as that of the two-way splitting FFD method, its total error is negligible for all azimuth angles. This means our optimized first-order compensation, compared with unoptimized first- and second-order compensations, has the highest accuracy for imaging steep dips with the lowest increase of computational cost.

Figure 2 shows relative phase error versus dip angle in diagonal direction. The three velocity contrasts $(v–v_0)/v$ used are of 70%, 50%, and 30%. For the three velocity contrasts listed, the error curves of three methods — two-way splitting FFD method, first-order compensation, and second-order compensation — increase gradually with increasing dip angles and exceed 1% at a dip angle of about 35°, 42°, and 48°, respectively. In contrast, the error curves of optimized first-order compensation oscillate under relative error of 1% and exceed 1% at dip angle of 60°.

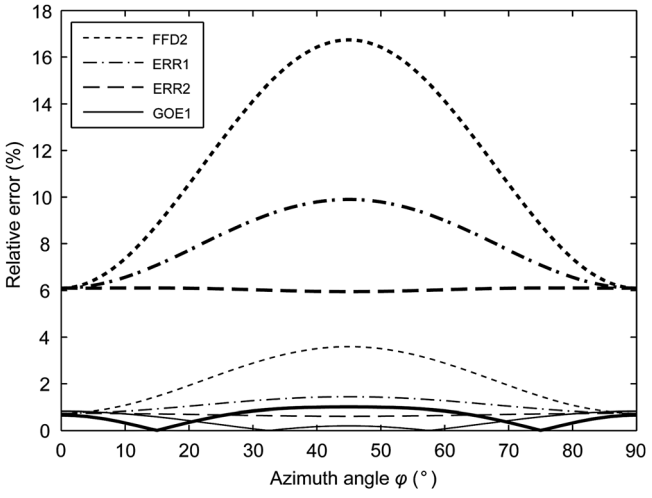

Figure 1. Relative error versus azimuth angle at two given dip angles. The velocity contrast $(v–v_0)/v$ used here is of 70%. There are two groups of lines listed in this figure. The thin and bold lines are corresponding to the dip angles of 45° and 60°, respectively. The short dashed lines represent the two-way splitting Fourier finite-difference method (denoted by FFD2). The dot dashed lines represent the method using first-order compensation after the two-way splitting Fourier finite-difference method (denoted by ERR1). The long dashed lines represent the method using second-order compensation after the two-way splitting Fourier finite-difference method (denoted by ERR2). The solid lines represent the globally optimized first-order compensation after the two-way splitting Fourier finite-difference method (denoted by GOE1). Note that the relative error of our globally optimized first-order compensation is never bigger than 1% for dip angles of 45° and 60°.

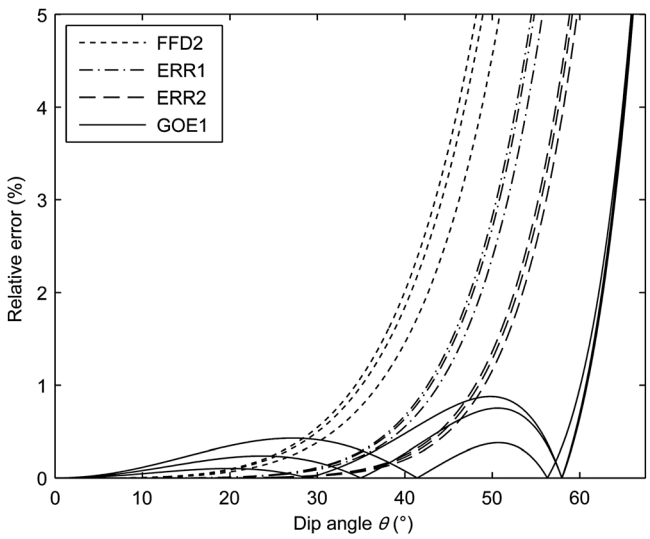

Figure 2. Relative error versus dip angle in diagonal direction. The three velocity contrasts $(v–v_0)/v$ used here are of 70%, 50%, and 30%. The short dashed lines represent the two-way splitting Fourier finite-difference method (denoted by FFD2). The dot dashed lines represent the method using first-order compensation after the two-way splitting Fourier finite-difference method (denoted by ERR1). The long dashed lines represent the method using second-order compensation after the two-way splitting Fourier finite-difference method (denoted by ERR2). The solid lines represent the globally optimized first-order compensation after the two-way splitting Fourier finite-difference method (denoted by GOE1).

Downloaded 10 Jun 2011 to 159.226.119.199. Redistribution subject to SEG license or copyright; see Terms of Use at http://segdl.org/

In other words, all these compensation methods can improve the accuracy over the dip range, but the optimized first-order compensation has the greatest improvement.

Figure 3 shows velocity contrast versus phase angle of the expanded square-root operator under relative error of 1%. The two-way splitting FFD method always shows the worst accuracy among all methods listed; the first-order compensation, second-order compensation and optimized first-order compensation have different improvements on it. Each curve has almost the same trend, and furthermore, all curves are nearly horizontal for the whole range of velocity contrasts except the range close to the weak velocity contrast area. This means all methods have a stable level of improvements for various velocity contrasts. For example, the accurate dip angle for a velocity contrast of 70% is about 35°, 42°, 48°, and 60°, respectively. Obviously, our optimized first-order compensation has the most significant improvement among these three compensations, at about 25°. This improvement is almost twice that of the second-order compensation.

Optimizing the second-order compensation can also greatly improve the accuracy with two additional Fourier transforms required, but its accurate dip angle is only about 64°, which is slightly higher than that of the optimized first-order compensation's 60°. Thus, we recommend using our optimized first-order compensation because it is a reasonable tradeoff between computational cost and phase accuracy.

Only the case in a diagonal direction is shown in Figure 3. If the accurate dip angle was found among all azimuth angles, the error curve of our optimized first-order compensation would show a slight fluctuation around the curve listed here. This is mainly because the maximum error may not always be located at diagonal directions like the other unoptimized methods (see Figure 1). But the general trend would be quite similar to the case in diagonal direction because the fluctuation is very limited only within a fixed error range of 1%.

NUMERICAL EXAMPLES

Migration impulse responses

In this section, we illustrate the theoretical accuracy analyses by impulse responses. A 3D homogeneous medium is defined on a grid system of $512 \times 512 \times 256$ with grid spacing of 10 m. A single input trace is located at the center of the upper surface. The traveltime is 500 ms with 2 ms sampling. The dominant frequency of a Ricker wavelet is 25 Hz. The real velocity is $v = 4500$ m/s with the reference velocity being $v_0 = 1500$ m/s (i.e., strong velocity contrast of $(v - v_0)/v \approx 70\%$). We use a tapered boundary of 15 traces along each side of the depth slab.

Figure 4 shows vertical slices of four methods: the two-way splitting FFD method, the first-order compensation, the second-order compensation, and the optimized first-order compensation. Each subfigure contains a left and right part, which are vertical profiles along inline and diagonal directions, respectively. Obviously, the first- and second-order compensations have no influence on the accuracy in inline and crossline directions. Their contributions are mainly around diagonal directions where there are significant two-way splitting errors. The angle shown on the right denotes the accurate dip angle in diagonal directions, which can be read from Figure 3. Figure 4c shows that the two-way splitting error is almost reduced completely under the dip angle of 48° because the accurate dip angle in diagonal directions (i.e., 47°) is close to that of those in inline and crossline directions (i.e., 48°).

Figure 4d shows that globally optimized first-order compensation can greatly reduce the two-way splitting error. The accurate dip angle in diagonal directions is now up to 60°, which is much higher than that of the unoptimized first-order compensation (42°). Meanwhile, we see that the accuracy in inline and crossline directions is preserved since the accurate dip angle in inline and crossline directions is still up to 70°.

Figure 5 shows depth slices of four methods: the two-way splitting FFD method, first-order compensation, second-order compensation, and optimized first-order compensation. Three depth levels are selected corresponding to dip angles of 45°, 60°, and 75°, respectively. Each subfigure contains four equivalent parts and each part corresponds to a method. Obviously, there is almost no splitting error at the dip angle of 45° since the wave fronts in all parts are close to theoretical positions (indicated by a dashed circle). At the dip angle of 60°, however, the two-way splitting error is significant for the two-way splitting FFD method, especially in diagonal directions where the wave fronts deviate from theoretical positions.

After using the first- and second-order compensations, the two-way splitting error is greatly reduced since the wave fronts appear to be much more circular. However, the wave fronts after the compensations are still not close to the theoretical positions. In contrast, the optimized first-order compensation produces a perfect circular response that is almost exactly on the theoretical position (see upper-right corner of each subfigure in Figure 5). Although the total error of our optimized first-order compensation

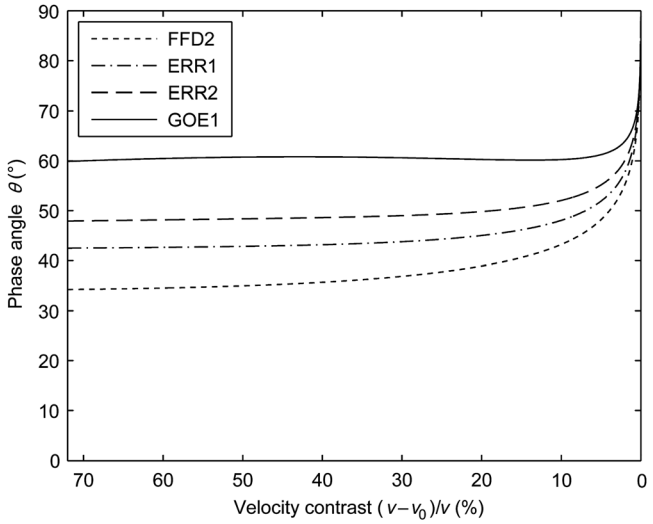

Figure 3. Velocity contrast versus dip angle in diagonal direction. The velocity contrast is defined as $(v-v_0)/v \times 100\%$. The dot dashed line represents the method using first-order compensation after the two-way splitting Fourier finite-difference method (denoted by ERR1). The long dashed line represents the method using second-order compensation after the two-way splitting Fourier finite-difference method (denoted by ERR2). The solid line represents the globally optimized first-order compensation after the two-way splitting Fourier finite-difference method (denoted by GOE1).

Downloaded 10 Jun 2011 to 159.226.119.199. Redistribution subject to SEG license or copyright; see Terms of Use at http://segdl.org/

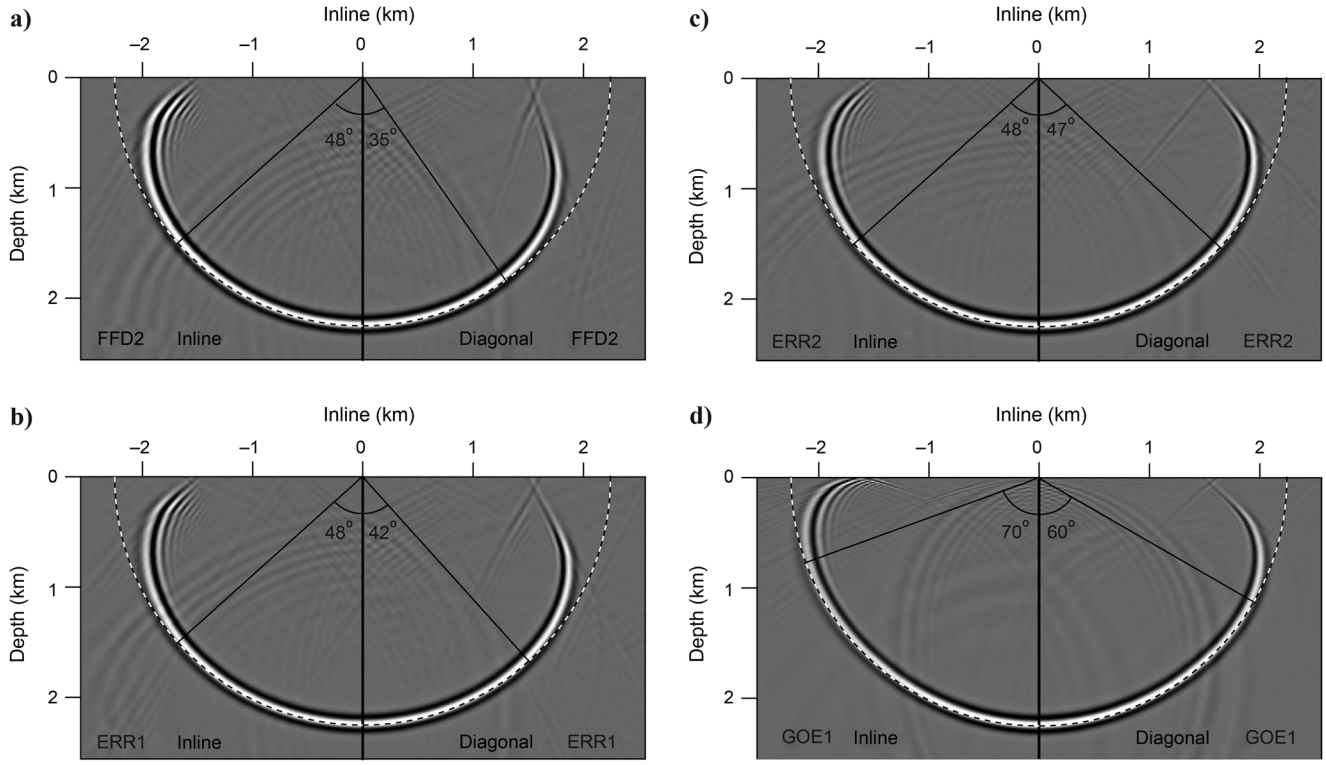

Figure 4. Vertical profiles at source location using different methods. (a) The two-way splitting Fourier finite-difference method (indicated by FFD2); (b) the first-order compensation after the two-way splitting Fourier finite-difference method (indicated by ERR1); (c) the second-order compensation after the two-way splitting Fourier finite-difference method (indicated by ERR2); (d) the globally optimized first-order compensation after the two-way splitting Fourier finite-difference method (indicated by GOE1). Each subfigure contains two parts: the left and right parts are vertical profiles along inline and diagonal directions, respectively. The dashed semicircle denotes the accurate position. The angle shown in the right part denotes the accurate dip angle in diagonal directions, which can be read from Figure 3. The real velocity of the homogeneous medium is v =4500 m/s, and the reference velocity for each panel is $v_0 = 1500$ m/s. The grid interval used in migration is 10 m. The dominant frequency of the Ricker wavelet is 25 Hz.

is still fairly large at the dip angle of 75°, the situation is much better than that of the unoptimized compensations.

Under the same hardware and software environments, the two-way splitting FFD method requires 1908.76 CPU seconds, whereas the three compensations — first-order compensation, second-order compensation, and optimized first-order compensation — require 2599.06, 3189.04, and 2623.51 CPU seconds, respectively. Compared with the two-way splitting FFD method, the increasing computational cost of the first-order compensation is about one-third of the cost; that of optimized first-order

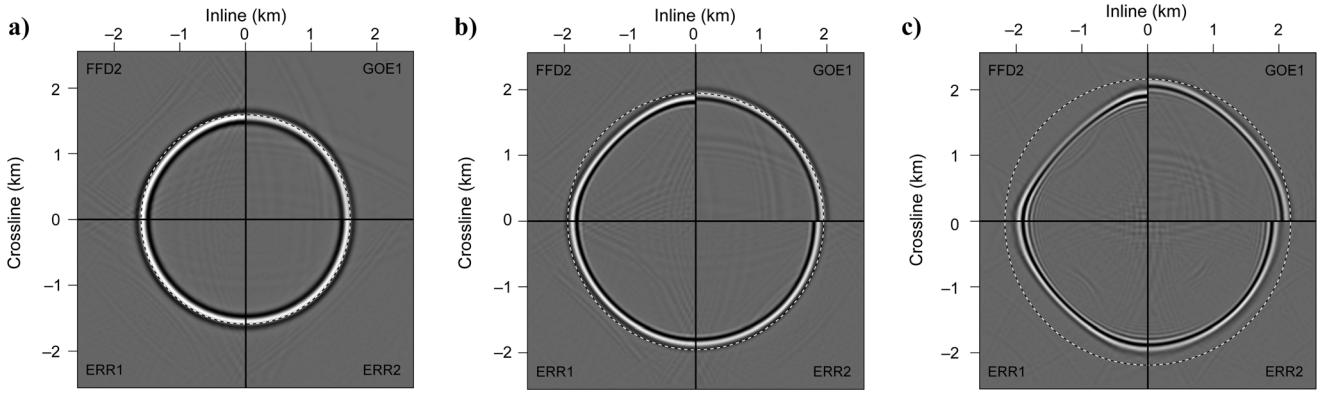

Figure 5. Depth slices of 3D impulse responses at different dip angles. (a) 45° (z=1590 m); (b) 60° (z=1125 m); (c) 75° (z=582 m). Each subfigure consists of four equivalent parts, and different parts use different methods. The left-upper quadrant shows FFD2, the left-bottom quadrant shows ERR1, the right-bottom quadrant shows ERR2, and the right-upper quadrant shows GOE1. The dashed circle denotes the accurate position. Parameters used here is the same as in Figure 4.

Downloaded 10 Jun 2011 to 159.226.119.199. Redistribution subject to SEG license or copyright; see Terms of Use at http://segdl.org/

compensation is also about one-third; and that of the second-order compensation is up to two-thirds. The increased computational cost of first-order compensation and optimized first-order compensation is very similar but the increased computational cost of second-order compensation is nearly twice that of first-order compensation.

Migration on SEG/EAGE salt

To verify the capabilities of three compensation methods on imaging 3D complex structures, we test the zero-offset migration problem (Ober et al., 1997) of the SEG/EAGE 3D salt model (Aminzadeh et al., 1996). The grid spacing is 40 m along the x- and y-directions and 20 m along depth direction. Eighty frequency components are extrapolated during migration. We use a tapered boundary of 15 traces along each side of the depth slab. In diagonal directions, the two-way splitting FFD method should have the worst accuracy among all azimuths. Thus, we extract the vertical slice along the diagonal direction at $x = y + 600$ m to illustrate the contributions of two-way splitting error compensation, as shown in Figure 6.

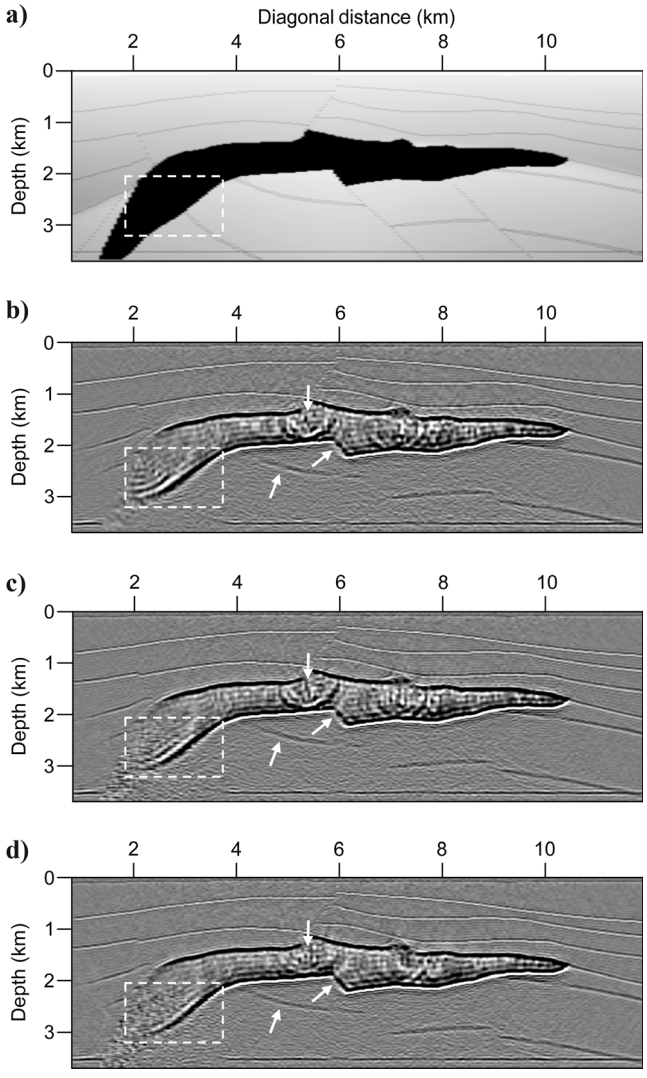

Figure 6. Vertical profiles along diagonal direction of 3D data sets. (a) SEG/EAGE salt model; (b) image result obtained by FFD2; (c) image result obtained by ERR1; (d) image result obtained by GOE1.

Generally, each method can well image the small-angle structures and even steep structures above the salt dome, but each method has a poor image for the left boundary of the salt root as well as the dipping structures under the salt. However, there are some significant improvements at the locations indicated by white arrows (see Figure 6). First, the optimized first-order compensation obtained a much sharper fault structure (see the position indicated by the middle white arrow) than the structure obtained by the two-way splitting FFD method and first-order compensation. Second, the optimized first-order compensation shows a much clearer image background within the salt dome (see the position indicated by the upper white arrow). Finally, the optimized first-order compensation shows a much more continuous subsurface under the salt dome (see the position indicated by the bottom white arrow).

In addition, there are also some significant improvements within the areas enclosed by rectangular boxes. For a detailed comparison, we zoom in on the images within the rectangular areas (see Figure 7). The bottom salt boundary was not well imaged by the two-way splitting FFD method because the image is far away from the correct position (indicated by the dashed line). Furthermore, there are relatively strong-energy parallel events left in the image, which are regarded as image artifacts. The first-order compensation can pull the image of the bottom salt boundary much closer to the correct position and reduces the image artifacts partially. In contrast, the optimized first-order compensation can locate the bottom salt boundary accurately and reduce the image artifacts completely. Figure 8 shows the depth slices at 2600 m. Similarly to the vertical slices shown in Figure 7, the two-way splitting FFD could not image the salt root very well, whereas the optimized first-order compensation can image the same target much better.

Under the same hardware and software environments, the two-way splitting FFD method runs for 383.83 CPU seconds, while the first-order compensation and the optimized first-order compensation run for 528.92 and 514.26 CPU seconds,

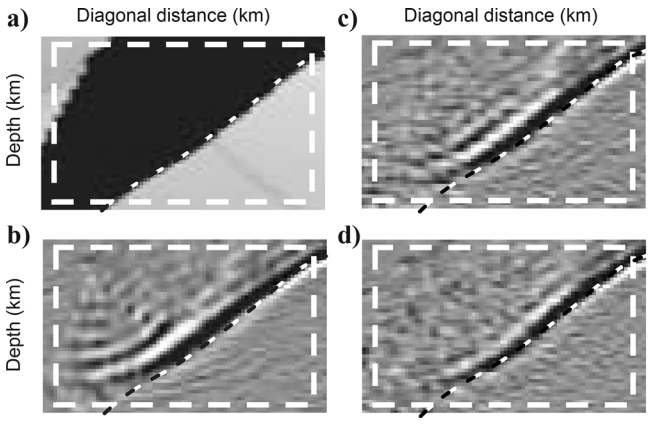

Figure 7. Comparison of the local details within the rectangular areas in Figure 6. The dashed line denotes the bottom salt boundary. (a) SEG/EAGE salt model; (b) image result obtained by FFD2; (c) image result obtained by ERR1; (d) image result obtained by GOE1.

Downloaded 10 Jun 2011 to 159.226.119.199. Redistribution subject to SEG license or copyright; see Terms of Use at http://segdl.org/

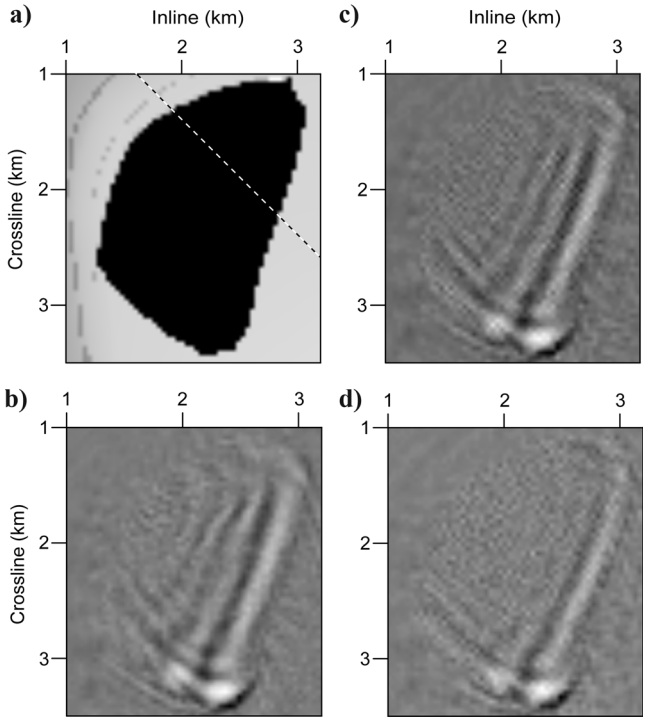

Figure 8. Comparison of depth slices at the salt root. (a) SEG/EAGE salt model; (b) image result obtained by FFD2; (c) image result obtained by ERR1; (d) image result obtained by GOE1. The slices are at the depth of 2600 m. The dashed line in (a) indicates the diagonal direction used in vertical profiles (Figure 6).

respectively. The increase of computational cost after using first-order compensation is about one-third, which is consistent with the previous numerical results.

DISCUSSIONS

During the optimization procedure, we found that the accuracy of the optimized operator is highly dependent on the optimization strategy. If all constants (about six) are optimized at the same time, the convergence is very slow, and it is difficult for us to obtain an excellent optimized operator. In our scheme, we first optimize a 2D FFD propagator and try to improve its accurate propagation angle. Then we substitute these 2D optimized coefficients into the 3D FFD operator and create a two-way splitting operator. Finally, we derive the compensation term and optimize its constant coefficients by optimizing the operator as a whole, where we need to relax the 2D optimized coefficients to improve the accuracy as much as possible. We only performed our optimization using a simulated annealing algorithm. We are not sure whether we can further improve the accuracy of our compensation by using other optimization methods (e.g., genetic algorithms).

The proposed compensation scheme can be applied to the finite-difference method to reduce two-way splitting error. But the contribution would be not as significant as it is in this paper. On the one hand, the two-way splitting error of the finite-difference method is much higher than that of the FFD method (Zhang et al., 2008); thus, a more powerful compensation is needed by the two-way splitting finite-difference method. On the other hand, the compensation scheme is limited to small two-way splitting error because there are two Taylor expansions involved during its operator expansion. Our numerical experiments suggest that the accurate dip angle obtained by optimized second-order compensation is only a few degrees (about 3°) higher than that obtained by the optimized first-order compensation. The contribution of the second-order compensation for the FFD method is so slight that we could not expect more for the finite-difference method.

The fast Fourier transform used in our code is a hybrid-radix algorithm. If we adopt a much faster implementation of Fourier transform (e.g., graphics card based parallel implementation, see Zhang et al., 2009a), the runtime proportion of Fourier transform would decrease rapidly. As a result, the increase in computational cost caused by adding Fourier transforms would be fairly minor. However, we could not further improve the accuracy even by using optimized second-order compensation. Thus, efforts should be directed to developing a more powerful method to compensate the two-way splitting error to obtain a circle response in a much higher wide-angle area (e.g., 70° or 80°).

Although we only show a zero-offset case, the main benefits will occur in prestack migration because much wider angles emerge when wavefields are propagating between sources and receivers. In addition, our scheme is not restricted to just the isotropic case. This method can help any medium which should have circular depth slice impulse responses, such as VTI media.

CONCLUSIONS

Wide-angle propagation is very important when using one-way wave equation methods to image complex structures. The two-way splitting FFD method is widely used because of its high computational efficiency and outstanding ability to image dipping structures in strong lateral velocity contrasts. However, the introduction of azimuthal anisotropy caused by two-way splitting diminishes the benefits of using the finite-difference scheme. This two-way splitting error will lead to large errors of image positions or even complete failure.

In this paper, we showed how to reduce the two-way splitting error using a dual-domain method. This method uses the basic idea of the traditional split-step Fourier method to reduce two-way splitting error rather than to reduce expanded error. It is a natural combination of the two-way splitting FFD method and the generalized-screen method. It adds a compensation term, similar to a high-order generalized-screen correction term, to reduce the two-way splitting error of the FFD method. Based on the globally optimized two-way splitting FFD method, our optimization scheme of the compensation part greatly improves the accurate propagation angle. Thus, it reduces computational cost caused by high-order corrections and requires only first-order compensation.

The most expensive parts of solving the two-way splitting FFD method are the two 2D Fourier transforms and an alternating-direction-implicit finite-difference scheme. After applying our compensation scheme, one additional 2D Fourier transform is required. Numerical experiments show that the increase of computational cost after using our compensation is only about one-third compared to the two-way splitting FFD method. The constraint on the accurate dip angle of traditional two-way splitting FFD method emerges in the diagonal directions, which is

Downloaded 10 Jun 2011 to 159.226.119.199. Redistribution subject to SEG license or copyright; see Terms of Use at http://segdl.org/

only about 35° under relative error of 1%. In contrast, after applying our compensation scheme, the accurate dip angle among all azimuths is at least 60°.

Compared with a purely wavenumber-domain method (a single-domain approach), our scheme is applicable to lateral velocity variations even in the case of strong velocity contrast. Compared with the spatial-domain finite-difference method, our scheme is much faster because it is solved by fast Fourier transforms. It naturally reduces to the traditional phase-shift method when the velocity becomes homogeneous. Thus, the compensation can be omitted when splitting error is small enough (e.g., for weak velocity contrasts or small dip angles). Our compensation scheme has a good tradeoff between computational cost and accurate propagation angle.

ACKNOWLEDGMENTS

We are grateful to John Etgen for his insightful suggestions and patient corrections, which greatly improve the quality and the legibility of our manuscript. We also thank anonymous reviewers for helpful comments and suggestions. This research was supported by the Major State Basic Research Development Program of China (973 Program) (Grant No. 2009CB219404), the National Natural Science Foundation of China (Grant No. 41074092), and the National Major Project of China (Grant No. 2011ZX05008-006).

REFERENCES

Aminzadeh, F., N. Burkhard, J. Long, T. Kunz, and P. Duclos, 1996, Three dimensional SEG/EAEG models — An update: The Leading Edge, **15**, 131–134, doi:10.1190/1.1437283.

Biondi, B., 2002, Stable wide-angle Fourier finite-difference downward extrapolation of 3-D wavefields: Geophysics, **67**, 872–882, doi:10.1190/1.1484530.

Brown, D. L., 1983, Applications of operator separation in reflection seismology: Geophysics, **48**, 288–294, doi:10.1190/1.1441468.

Claerbout, J. F., 1985, Imaging the earth's interior: Blackwell Scientific Publications, Inc.

Collino, F., and P. Joly, 1995, Splitting of operators, alternate directions, and paraxial approximations for the three-dimensional wave equation: SIAM Journal on Scientific Computing, **16**, 1019–1048, doi:10.1137/0916059.

de Hoop, M. V., J. H. Le Rousseau, and R. S. Wu, 2000, Generalization of the phase-screen approximation for the scattering of acoustic waves: Wave Motion, **31**, 43–70, doi:10.1016/S0165-2125(99)00026-8.

Douglas, J., 1962, Alternating direction methods for three space variables: Numerische Mathematik, **4**, 41–63, doi:10.1007/BF01386295.

Etgen, J., S. H. Gray, and Y. Zhang, 2009, An overview of depth imaging in exploration geophysics: Geophysics, **74**, no. 6, WCA5–WCA17, doi:10.1190/1.3223188.

Fei, T. W., and J. T. Etgen, 2002, Domain decomposition for 3-D finite-difference depth extrapolation: 72nd Annual International Meeting, SEG, Expanded Abstracts, 1160–1163.

Gazdag, J., 1978, Wave equation migration with the phase-shift method: Geophysics, **43**, 1342–1351, doi:10.1190/1.1440899.

Gazdag, J., and P. Sguazzero, 1984, Migration of seismic data by phase shift plus interpolation: Geophysics, **49**, 124–131, doi:10.1190/1.1441643.

Graves, R. W., and R. W. Clayton, 1990, Modeling acoustic waves with paraxial extrapolation: Geophysics, **55**, 306–319, doi:10.1190/1.1442838.

Huang, L. J., and M. C. Fehler, 2000, Globally optimized Fourier finite-difference migration method: 70th Annual International Meeting, SEG, Expanded Abstracts, 802–805.

Jin, S., R. S. Wu, and C. Peng, 1999, Seismic depth migration with pseudo-screen propagator: Computational Geosciences, **3**, 321–335, doi:10.1023/A:1011587227696.

Kirkpatrick, S., C. D. Gelatt, and M. P. Vecchi, 1983, Optimization by simulated annealing: Science, **220**, 671–680, doi:10.1126/science.220.4598.671.

Lee, M. W., and S. Y. Suh, 1985, Optimization of one-way wave equations: Geophysics, **50**, 1634–1637, doi:10.1190/1.1441853.

Le Rousseau, J. H., and M. V. de Hoop, 2001, Modeling and imaging with the scalar generalized-screen algorithms in isotropic media: Geophysics, **66**, 1551–1568, doi:10.1190/1.1487101.

Li, Z., 1991, Compensating finite-difference errors in 3-D migration and modeling: Geophysics, **56**, 1650–1660, doi:10.1190/1.1442975.

Liu, L., and J. Zhang, 2006, 3D wavefield extrapolation with optimum split-step Fourier method: Geophysics, **71**, no. 3, T95–T108, doi:10.1190/1.2197493.

Ober, C. C., R. A. Oldfield, D. E. Womble, and C. C. Mosher, 1997, Seismic imaging on massively parallel computers: 67th Annual International Meeting, SEG, Expanded Abstracts, 1418–1421.

Peaceman, D.W., and H.H. Rachford Jr., 1955, The numerical solution of parabolic and elliptic differential equations: SIAM Journal on Applied Mathematics, **3**, 28–41, doi:10.1137/0103003.

Rickett, J., J. Claerbout, and S. Fomel, 1998, Implicit 3-D depth migration by wavefield extrapolation with helical boundary conditions: 68th Annual International Meeting, SEG, Expanded Abstracts, 1124–1127.

Ristow, D., and T. Rühl, 1994, Fourier finite-difference migration: Geophysics, **59**, 1882–1893, doi:10.1190/1.1443575.

Ristow, D., and T. Rühl, 1997, 3-D implicit finite-difference migration by multiway splitting: Geophysics, **62**, 554–567, doi:10.1190/1.1444165.

Stoffa, P. L., J. T. Fokkema, R. M. de Luna Freire, and W. P. Kessinger, 1990, Split-step Fourier migration: Geophysics, **55**, 410–421, doi:10.1190/1.1442850.

Wachspress, E. L., and G. J. Habetler, 1960, An alternating-direction-implicit iteration technique: SIAM Journal on Applied Mathematics, **8**, 403–424, doi:10.1137/0108027.

Wang, Y., 2001, ADI plus interpolation: Accurate finite-difference solution to 3D paraxial wave equation: Geophysical Prospecting, **49**, 547–556, doi:10.1046/j.1365-2478.2001.00278.x.

Wu, R. S., 1994, Wide-angle elastic wave one-way propagation in heterogeneous media and an elastic wave complex-screen method: Journal of Geophysics Research, **99**, 751–766, doi:10.1029/93JB02518.

Wu, R. S., 2003, Wave propagation, scattering and imaging using dual-domain one-way and one-return propagators: Pure and Applied Geophysics, **160**, 509–539, doi:10.1007/PL00012548.

Xie, X. B., and R. S. Wu, 1999, Improving the wide angle accuracy of screen propagator for elastic wave propagation: 69th Annual International Meeting, SEG, Expanded Abstracts, 1863–1866.

Xie, X. B., and R. S. Wu, 2001, Modeling elastic wave forward propagation and reflection using the complex screen method: Journal of the Acoustical Society of America, **109**, 2629–2635, doi:10.1121/1.1367248.

Zhang, J., and L. Liu, 2007, Optimum split-step Fourier 3D depth migration: Developments and practical aspects: Geophysics, **72**, no. 3, S167–S175, doi:10.1190/1.2715658.

Zhang, J. H., W. M. Wang, L. Y. Fu, and Z. X. Yao, 2008, 3D Fourier finite-difference migration by alternating-direction-implicit plus interpolation: Geophysical Prospecting, **56**, 95–103, doi:10.1111/j.1365-2478.2007.00656.x.

Zhang, J. H., S. Q. Wang, and Z. X. Yao, 2009a, Accelerating 3D Fourier migration with graphics processing units: Geophysics, **74**, no. 6, WCA129–WCA139, doi:10.1190/1.3223186.

Zhang, J. H., W. M. Wang, and Z. X. Yao, 2009b, Comparison between the Fourier finite-difference method and the generalized-screen method: Geophysical Prospecting, **57**, 355–365, doi:10.1111/j.1365-2478.2008.00748.x.

Zhang, J. H., W. M. Wang, S. Q. Wang, and Z. X. Yao, 2010, Optimized Chebyshev Fourier migration: A wide-angle dual-domain method for media with strong velocity contrasts: Geophysics, **75**, no. 2, S23–S34, doi:10.1190/1.3350861.

Zhu, S. W., J. H. Zhang, and Z. X. Yao, 2008, Globally optimized Fourier finite-difference operator using simulated annealing algorithm based on multi-parameter: Chinese Journal of Geophysics (in Chinese), **51**, 1844–1850.

Downloaded 10 Jun 2011 to 159.226.119.199. Redistribution subject to SEG license or copyright; see Terms of Use at http://segdl.org/